An Investigation of the BCP Potential Energy Surface

Hyun Joo and Michael L. McKee*

Department of Chemistry, Auburn University, Auburn, Alabama 36849

Received: October 16, 2003; In Final Form: December 23, 2003

The singlet and triplet potential energy surfaces (PESs) of boron−carbon−phosphorus (BCP) isomers were investigated, using various theoretical methods. Geometries of the minima and transition states on the PES were optimized at the B3LYP/6-311+G(2df) and CASSCF(12,12)/6-311+G(2df) levels, and single-point calculations were made at the CASPT2/ANO-L level, to consider dynamic electron correlation effects. The most-stable isomer was linear singlet BCP ($^1\Sigma^+$); its calculated heat of formation ($\Delta_f H°$, 0 K) is 150.5 ± 2 kcal/mol. Study of the fragmentation processes in BCP revealed that the bond enthalpies of the B−C and C−P bonds in BCP ($^1\Sigma^+$) at 0 K are 111.7 and 128.9 kcal/mol, respectively, at the CASPT2/ANO-L level. A possible crossing mechanism between two electronic states ($^3A'$ and $^3A''$) is discussed, and Renner−Teller species with $^3\Pi$ state symmetry are investigated.

Introduction

The physical properties of nanomaterials are affected by the nature of the constitutent elements, their composition, and their crystalline structure. A great amount of attention has been given to group 13, 14, and 15 elements, because they have the same number of valence electrons as materials that have already been developed and are widely used in industry. Furthermore, there has been much interest in materials composed of boron, carbon, and nitrogen (BCN), because they are expected to have useful properties as semiconductors, batteries, etc.[1−6] In addition, BCN compounds are known to possess tunable band gaps by changing the elemental composition and by adapting different synthetic methods, which lead to different crystalline structures. Even though many theoretical studies of BCN are available,[7−10] to our knowledge, no experimental or theoretical study of the boron−carbon−phosphorus (BCP) molecule, which is isoelectronic to C_3 and BCN, has been reported. Because of the similarity of the electronic structures, BCP can be expected to possess physical properties that are similar to those of BCN, which piqued our interest.

BCP can be formed through the reaction of a diatomic with an atom, such as boron carbide (BC) + phosphorus, boron + carbon phosphide (CP), and carbon + boron phosphide (BP). Although both diatomic molecules BC and CP have been observed, BC is best known both theoretically and experimentally.[11−20] Using mass spectrometry, Drowart and co-workers determined that BC has a bond dissociation energy (BDE) of 105 ± 10 kcal/mol.[11,12] Kuoba and Öhrn[13] established the ground state for BC as $^4\Sigma^-$, with the major configuration $1\sigma^2 2\sigma^2 3\sigma^2 4\sigma^2 5\sigma 1\pi^2$. Fernando et al. obtained various spectroscopic parameters, including the equilibrium bond length (r_e = 1.491 Å), by studying gas-phase emission spectra of BC.[14] Recently, Tzeli and Mavridis reported multireference configuration interaction (MRCI) calculations, using a complete basis limit extrapolation, and argued that their value for D_e (102.2 ± 0.1 kcal/mol) was more accurate than the experimental value (108 ± 7 kcal/mol).[20] BP is another interesting boron compound; it can be made into semiconducting thin films via chemical vapor deposition.[21] The electronic structure and band gaps of BP polymers have been studied;[22−24] however, investigations of monomeric BP are rare. Interest in CP has been sparked by the discovery of CP in the inner layers of the carbon star envelope IRC+10216.[25] In addition, a serious deviation between the calculated heat of formation ($\Delta_f H°$) of CP and the experimental values in the NIST Webbook has been discovered.[26−28] Now, it is accepted that the recommended value for $\Delta_f H°$ (0 K) of CP is ∼124 kcal/mol, rather than 106 kcal/mol.

We report herein a comprehensive study on the singlet and triplet potential energy surfaces (PESs) of the hypothetical BCP molecule, using DFT, CASSCF, and CASPT2 methods. Various spectroscopic and thermodynamic parameters are also calculated at each level. For the linear triatomic species that have degenerate electronic states ($^3\Pi$), Renner−Teller (RT) effects were examined, using harmonic vibrational frequency analysis.

Computational Details

The Gaussian98 program[29] was used for density functional UB3LYP[30] calculations, the GAMESS program[31] was used for complete active space SCF (CASSCF)[32] calculations, and the MOLCAS 5.4[33] was applied for CAS calculations with dynamic electron correlation introduced at the MP2 level (CASPT2).[34] All calculations were performed on a cluster of Linux computers. Geometry optimizations for the minima and transition states were conducted at the UB3LYP and full-valence CASSCF-(12,12) levels with the 6-311+G(2df) basis set.[35] Further stability tests and wave function optimizations were performed to determine spin-broken symmetry solutions at the UB3LYP level. According to harmonic vibrational frequency analyses, each stationary structure was characterized as a minimum (no imaginary frequencies) or a transition state (one imaginary frequency) at the UB3LYP/6-311+G(2df) level. Zero-point vibrational energies and heat-capacity corrections were obtained from UB3LYP/6-311+G(2df) frequency calculations. On the triplet PES, there were intruder state problems, which were solved by applying the level shift (LS) technique.[36] Transition

* Author to whom correspondence should be addressed. E-mail: mckee@chem.auburn.edu.

10.1021/jp031170b CCC: $27.50 © 2004 American Chemical Society
Published on Web 02/11/2004

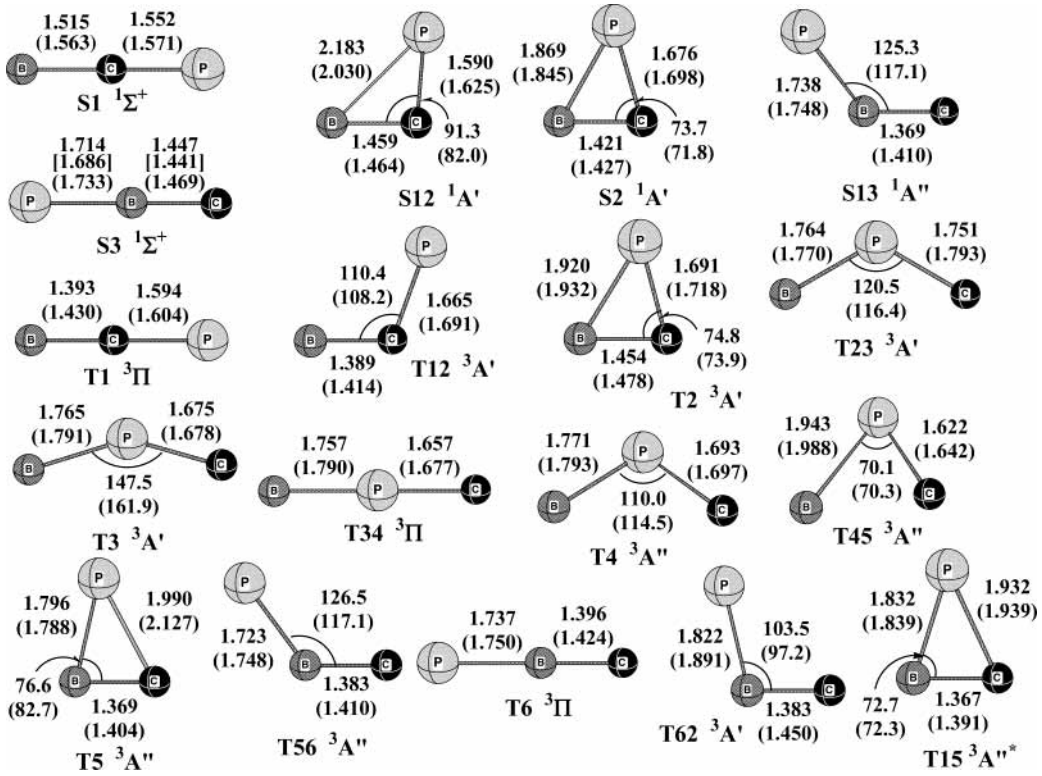

Figure 1. Optimized geometric parameters of stationary points at the DFT level (values in parentheses are data from the CAS level). Bond lengths are given in angstroms, and angles are given in degrees. The asterisk symbol (*) indicates that the geometry was obtained at the DFT level using the 6-311+G(df) basis set. The square brackets for **S3** indicate values that were obtained with RDFT (i.e., **S3′**).

vectors of the transition states were visualized and animated by the MOLDEN program,[37] to ensure that the motions were as expected.

For triplet linear isomers, vibrational frequencies at the CASSCF(12,12)/6-311+G(2df) level were also calculated, to investigate the Renner−Teller effect.[38] Dynamic electron correlation was considered by means of single-point full-valence CASPT2 calculations for every stationary point calculated at the CASSCF(12,12)/6-311+G(2df) level with the ANO-L basis set,[39] which is a [7s7p5d4f] contraction of the [17s12p5d4f] primitive set for the P atom and a [7s7p4d3f] contraction of the [14s9p4d3f] primitive set for the B and C atoms. *Note: Throughout this paper, we will refer to UB3LYP/6-311+G(2df) as DFT, CASSCF(12,12)/6-311+G(2df) as CAS, and CASPT2-(12,12)/ANO-L//CASSCF(12,12)/6-311+G(2df) as CASPT2, respectively*. In the GAMESS and MOLCAS calculations, the C_{2v} point group was adapted for linear isomers, because of the limitations in handling high symmetry. The geometry of the conical intersection was obtained at the CASSCF(6,6)/6-311+G-(2df) level, using Gaussian98, and then single-point calculations for both electronic states (^{3}A′ and ^{3}A″) were performed at the CAS level with GAMESS and at the CASPT2 level with MOLCAS. The natural bonding orbital (NBO)[40] program implemented in the Gaussian98 program was used for the Wiberg bond index (WBI)[41] analysis. Thermodynamic and spectroscopic properties were calculated from the DFT and CASPT2 results by methods that have been referenced in the literature.[42] For comparison, we also performed G3B3[43] calculations to obtain the heat of formation of the **S1** isomer (Figure 1). We will use a boldface notation scheme, with a boldface "**S**" for singlets and a boldface "**T**" for triplets, followed by one number for minima and two numbers for transition states. Thus, "**T12**" is the triplet transition state between triplet **T1** and triplet **T2**.

Results and Discussion

Important electronic configurations of the diatomic fragments and minimum energy species of BCP species are given in Table 1. For the diatomic fragments, only ground states are considered. The ground-state electronic configurations of BC and CP are available from the literature, and we obtained the same configurations for the ground states of BC ($^4\Sigma^-$) and CP ($^2\Sigma^+$). The ground state of BP is $^3\Pi$ with the electronic configuration [Core]$5\sigma^2 6\sigma^2 2\pi^3 7\sigma$, which is the same as that previously reported.[44,45] This observation suggests that BP can be obtained by combining ground-state B and P atoms without changing the electronic configuration. This fact can help explain why BP can easily polymerize to form a polymeric film (boron phosphide), because the diradical is expected to be kinetically labile.[21]

The ground state of the linear BCP (**S1**), the first excited linear triplet isomer (**T1**), and other linear isomers have the following electronic configurations:

$$[\text{Core}]6\sigma^2 7\sigma^2 8\sigma^2 2\pi^4 9\sigma^2 \qquad \text{(for } \mathbf{S1}\ (^1\Sigma^+) \text{ and } \mathbf{S3}\ (^1\Sigma^+))$$

$$[\text{Core}]6\sigma^2 7\sigma^2 8\sigma^2 2\pi^4 9\sigma 3\pi$$

(for **T1** ($^3\Pi$), **T6** ($^3\Pi$), and **T34** ($^3\Pi$))

Triangular C_s symmetry isomers have the following electronic configurations:

$$[\text{Core}]7a'^2 8a'^2 9a'^2 10a'^2 2a''^2 11a'^2 \qquad \text{(for } \mathbf{S2}\ (^1\text{A}'))$$

$$[\text{Core}]7a'^2 8a'^2 9a'^2 10a'^2 2a''^2 11a'12a'$$

(for **T2** and **T3** (^{3}A′))

$$[\text{Core}]7a'^2 8a'^2 9a'^2 10a'^2 2a''^2 11a'3a''$$

(for **T4** and **T5** (^{3}A″))

TABLE 1: Important Electronic Configurations of Ground-State Diatomic Fragments of BCP and Minimum-Energy Isomers of BCP at the CASPT2 Level[a]

configurations	C_i^2
BC, $^4\Sigma^-$ ($^4A_2$)	
$3\sigma^2 4\sigma^2 5\sigma 1\pi_x 1\pi_y$	0.89
$3\sigma^2 4\sigma 5\sigma^2 1\pi_y 2\pi_x$	0.02
$3\sigma^2 4\sigma 5\sigma^2 1\pi_x 2\pi_y$	0.02
CP, $^2\Sigma^+$ ($^2A_1$)	
$5\sigma^2 6\sigma^2 2\pi^4 7\sigma$	0.85
$5\sigma^2 6\sigma^2 2\pi_x{}^2 7\sigma 3\pi_y{}^2$	0.02
$5\sigma^2 6\sigma^2 2\pi_y{}^2 7\sigma 3\pi_x{}^2$	0.02
$5\sigma^2 6\sigma^2 2\pi_x{}^2 1\bar{\pi}_y 7\sigma 3\pi_y$	0.01
$5\sigma^2 6\sigma^2 2\bar{\pi}_x 1\pi_y{}^2 7\sigma 3\pi_x$	0.01
BP, $^3\Pi$ ($^3B_1$)	
$5\sigma^2 6\sigma^2 2\pi_x 2\pi_y{}^2 7\sigma$	0.90
$5\sigma^2 6\sigma^2 2\pi_x 7\sigma 3\pi_y{}^2$	0.02
S1, $^1\Sigma^+$ ($^1A_1$)	
$6\sigma^2 7\sigma^2 8\sigma^2 2\pi^4 9\sigma^2$	0.82
$6\sigma^2 7\sigma^2 8\sigma^2 2\pi^4 3\pi_x 4\bar{\pi}_x$	0.01
$6\sigma^2 7\sigma^2 8\sigma^2 2\pi^4 3\pi_y 4\bar{\pi}_y$	0.01
$6\sigma^2 7\sigma^2 8\sigma^2 2\pi_x{}^2 9\sigma^2 3\pi_y{}^2$	0.01
$6\sigma^2 7\sigma^2 8\sigma^2 2\pi_y{}^2 9\sigma^2 3\pi_x{}^2$	0.01
$6\sigma^2 7\sigma^2 8\sigma^2 2\pi_x 2\pi_y 9\sigma^2 3\bar{\pi}_x 3\bar{\pi}_y$	0.01
S2, $^1A'$	
$7a'^2 8a'^2 9a'^2 10a'^2 2a''^2 11a'^2$	0.78
$7a'^2 8a'^2 9a'^2 10a'^2 2a''^2 12a'^2$	0.08
$7a'^2 8a'^2 9a'^2 10a'^2 11a'^2 3a''^2$	0.01
S3, $^1\Sigma^+$ ($^1A_1$)	
$6\sigma^2 7\sigma^2 8\sigma^2 2\pi^4 9\sigma^2$	0.73
$6\sigma^2 7\sigma^2 8\sigma^2 2\pi_y{}^2 9\sigma^2 3\pi_x{}^2$	0.05
$6\sigma^2 7\sigma^2 8\sigma^2 2\pi_x{}^2 9\sigma^2 3\pi_y{}^2$	0.05
$6\sigma^2 7\sigma^2 8\sigma^2 2\pi_x 2\pi_y 9\sigma^2 3\bar{\pi}_x 3\bar{\pi}_y$	0.03
$6\sigma^2 7\sigma^2 8\sigma^2 2\pi_x 2\bar{\pi}_y 9\sigma^2 3\pi_x 3\bar{\pi}_y$	0.02
$6\sigma^2 7\sigma^2 8\sigma^2 2\pi_x{}^2 2\pi_y 9\sigma^2 3\bar{\pi}_y$	0.01
$6\sigma^2 7\sigma^2 8\sigma^2 2\pi_x 2\pi_y{}^2 9\sigma^2 3\bar{\pi}_x$	0.01
T1, $^3\Pi$ ($^3B_1$)	
$6\sigma^2 7\sigma^2 8\sigma^2 2\pi^4 9\sigma 3\pi_x$	0.85
$6\sigma^2 7\sigma^2 8\sigma^2 2\pi_x{}^2 9\sigma 3\pi_x 3\pi_y{}^2$	0.02
T2, $^3A'$	
$7a'^2 8a'^2 9a'^2 10a'^2 2a''^2 11a'12a'$	0.86
$7a'^2 8a'^2 9a'^2 10a'^2 11a'12a'3a''^2$	0.01
T3, $^3A'$	
$7a'^2 8a'^2 9a'^2 10a'^2 2a''^2 11a'12a'$	0.79
$7a'^2 8a'^2 9a'^2 10a'^2 11a'12a'3a''^2$	0.01
T4, $^3A''$	
$7a'^2 8a'^2 9a'^2 2a''^2 10a'^2 11a'3a''$	0.80
$7a'^2 8a'^2 9a'^2 2a'' 10a'^2 11a'3\bar{a}''4a''$	0.01
T5, $^3A''$	
$7a'^2 8a'^2 9a'^2 2a''^2 10a'^2 11a'3a''$	0.80
$7a'^2 8a'^2 9a'^2 2a''^2 10a'^2 11a'^2 3a''$	0.01
T6, $^3\Pi$ ($^3B_1$)	
$6\sigma^2 7\sigma^2 8\sigma^2 2\pi^4 9\sigma 3\pi_x$	0.69
$6\sigma^2 7\sigma^2 8\sigma^2 2\pi_x{}^2 9\sigma 3\pi_x 3\pi_y{}^2$	0.06
$6\sigma^2 7\sigma^2 8\sigma^2 2\pi_x{}^2 2\bar{\pi}_y 9\sigma 3\pi_x 3\pi_y$	0.03
$6\sigma^2 7\sigma^2 8\sigma^2 2\pi_x 2\bar{\pi}_y 9\sigma 3\pi_x{}^2 3\pi_y$	0.02
$6\sigma^2 7\sigma^2 8\sigma^2 2\pi_x{}^2 2\pi_y 9\sigma 3\pi_x 3\bar{\pi}_y$	0.01
$6\sigma^2 7\sigma^2 8\sigma^2 2\pi_x{}^2 2\pi_y 9\sigma 3\bar{\pi}_x 3\pi_y$	0.01

[a] Orbitals with a single β-spin electron are indicated with a bar over the orbital designation.

Excitation from the singlet state to the triplet state can be accomplished by exciting one electron from the highest occupied molecular orbital (HOMO, 9σ) to the lowest unoccupied molecular orbital (LUMO, 3π). The other linear isomer on the singlet PES (CBP), **S3**, also has the same configuration as **S1**, and two triplet linear species (CBP, BPC), **T6** and **T34**, have the same configuration as **T1**. In our calculations for the triplet linear, using the C_{2v} point group, we only calculate one component of the degenerate triplet state; however, we give the linear electronic state designation in Table 1. Linear species have some multireference character, as judged by the square of the coefficient of the dominant configuration to the wave function (C_i^2), which is 0.69−0.85 (see Table 1). The low-lying π-orbitals ($2\pi/3\pi/4\pi$) are important in this system, where four to six electrons are distributed among the π sets.

SCHEME 1: Lewis Structures of S1 and T1

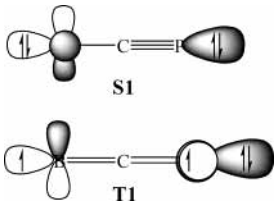

All possible linkage isomers of three atoms on singlet and triplet surfaces were considered. Optimized structures are as shown in Figure 1, and their relative energies are given in Table 2. Three singlet and six triplet minimum energy structures are characterized from the DFT geometry optimizations and frequency calculations. Among those isomers, singlet linear B−C−P (**S1**) with the $^1\Sigma^+$ electronic state proved to be the global minimum.

For most structures, geometries that were optimized at the CAS level had slightly longer bond lengths than those at the DFT level (see Figure 1), because of the population of antibonding orbitals. The B−C bond lengths in **S1** and **T1** isomers showed larger deviations between DFT and CAS that may be attributed to the neglect of dynamic electron correlations in the CASSCF method.

In **S1** (BCP), the C−P bond is a triple bond (1.552 Å, DFT) and is slightly shorter than the experimental bond length of CP (1.562 Å),[46] whereas the B−C bond is a single bond (1.515 Å, DFT) and is slightly longer than the experimental bond length in BC (1.491 Å).[14] The C−P and B−C bond lengths (1.594 and 1.393 Å, DFT) in **T1** (BCP) are longer and shorter than a normal CP triple bond and a normal BC single bond, respectively. These bond length changes can be easily rationalized by drawing Lewis structures of **S1** and **T1**. As shown in Scheme 1, the triplet **T1** is formed from **S1** by promoting an electron from the lone pair of B into an empty π*-orbital of P. The CP bond in **T1** becomes weaker while the BC bond becomes stronger. At the CASPT2+ZPC level, **T1** is 16.3 kcal/mol less stable than **S1**.

Three triangular planar structures—**S2**, **T2**, and **T5**—are found to be the minima, and their electronic states are $^1A'$, $^3A'$, and $^3A''$, respectively. **S2** and **T2** have very similar geometries, and their energy difference is only 2.2 kcal/mol at the CASPT2+ZPC level. Therefore, it is possible that vibrational excitation may lead to intersystem crossing. The other triangular isomer (**T5**) has a somewhat different structure from **S2** and **T2**, with a much longer P−C bond (1.990 Å). All three isomers have relatively low energies, despite high bond strain, which may be attributed to the large size of the P atom and the relatively weak repulsion among the electron pairs around the P atom.

Another pair of linear linkage isomers, **S3**/**T6** (PBC), exhibits properties that are very similar to those of **S1**/**T1** (PCB), where the BC fragment is rotated by 180°. The triplet (**T6**) can be formed from **S3** by promoting a P lone-pair electron to an empty C π*-orbital, which, in turn, can form a partial B−C double bond. Thus, the B−C bond is shorter in **T6** (1.396 Å) than in **S3 (**1.447 Å**)**, but the P−B bond is longer in T6 (1.737 Å) than in S3 (1.714 Å).

TABLE 2: Relative Energies of Species on the Potential Energy Surface of BCP

BCP	state	$\langle S^2\rangle^a$	Rw[b]	ZPC[a] (kcal/mol)	H_{corr}[a] (kcal/mol)	ΔE (kcal/mol)			ΔE + ZPC (kcal/mol)		
						DFT	CAS	CASPT2	DFT	CAS	CASPT2
S1	$^1\Sigma^+$	0.15	0.91	3.6	6.6	0.0	0.0	0.0	0.0	0.0	0.0
S2	$^1A'$	0.72	0.90	4.0	6.6	12.4	24.7	13.6	12.8	25.1	14.0
S3[c]	$^1\Sigma^+$	0.56	0.90	3.4	6.5	35.6	42.4	35.6	35.4	42.2	35.4
S3′[c]	$^1\Sigma^+$	0.00		3.3	5.5	37.2			36.9		
S12	$^1A'$	0.29	0.90	3.0	5.4	19.8	29.7	19.4	19.2	29.1	18.8
S13	$^1A''$	1.10	0.89	3.3	5.7	63.0	83.8	70.3	62.8	83.6	70.0
T1	$^3\Pi$	2.02	0.90	4.3	7.0	11.2	19.7	15.6	11.9	20.4	16.3
T2	$^3A'$	2.01	0.88	4.0	6.5	15.1	28.3	15.8	15.5	28.7	16.2
T3	$^3A'$	2.06	0.89	2.5	5.5	93.5	97.6	91.2	92.5	96.6	90.2
T4	$^3\Pi$	2.08	0.90	3.1	5.5	87.6	93.3	88.5	87.1	92.8	88.0
T5	$^3A''$	2.03	0.88	3.5	6.3	50.2	61.2	49.2	50.1	61.1	49.1
T6	$^3A''$	2.46	0.89	3.7	6.5	52.5	59.2	52.1	52.7	59.4	52.3
T12	$^3A'$	2.01	0.87	3.5	5.9	30.9	43.4	34.0	30.9	43.4	33.9
T23	$^3A'$	2.03	0.89	2.2	4.7	94.9	103.2	95.2	93.6	101.9	93.8
T34	$^3\Pi$	2.05	0.89	2.5	4.6	93.9	97.7	91.0	92.8	96.6	89.9
T45	$^3A''$	2.38	0.90	2.0	4.6	99.1	102.1	99.8	97.6	100.5	98.3
T56[d]	$^3A''$	2.11	0.89	3.3	5.7	56.4	64.1	55.5	56.1	63.9	55.2
T15[e]	$^3A''$	2.03	0.91	3.2	5.6	50.2	81.3	48.2	49.8	80.9	48.7
T26[e]	$^3A'$	2.06	0.91	3.0	5.5	73.7	79.4	66.3	73.1	78.8	66.6
$\mathbf{T_{crs}}$[f]				3.1	5.5		96.1	91.4		95.7	91.0

[a] Spin-squared values $\langle S^2\rangle$, zero-point corrections (ZPC), and heat-capacity contributions to enthalpy at 298 K (H_{corr}) were calculated at the B3LYP/6-311+G(2df) level. [b] Reference weight, which is the fraction of electron correlation energy obtained within the active space; Rw values were calculated at the CASPT2(12,12)/ANO-L//CASSCF(12,12)/6-311+G(2df) level. [c] The **S3** species is determined by UDFT (broken-symmetry), whereas **S3′** is determined by RDFT (closed-shell). **S3** is a minimum, whereas **S3′** is a transition state. [d] DFT results were obtained using B3LYP/6-311+G(df) geometry optimization with a single-point calculation at the B3LYP/6-311+G(2df) level. [e] CASPT2 results were obtained using the level shift (LS) method (see Table 3). [f] The geometry of the crossing point was obtained at the CASSCF(6,6)/6-311+G(2df) level. The ZPC from **T4** was used to compute the values under "ΔE + ZPC".

TABLE 3: Energies Relative to T2 (ΔE) and Reference Weights (Rw) Obtained Using the Level Shift (LS) Technique[a]

	T1		**T15**		**T5**		**T2**		**T26**		**T6**	
LS	ΔE (kcal/mol)	Rw	ΔE (kcal/mol)	Rw	ΔE (kcal/mol)	Rw	ΔE (kcal/mol)	Rw	ΔE (kcal/mol)	Rw	ΔE (kcal/mol)	Rw
0.0	1.0	0.90	33.7	0.15	33.8	0.88	0.0	0.88	49.8	0.34	37.0	0.89
0.1	1.0	0.91	32.4	0.90	33.9	0.90	0.0	0.91	44.0	0.82	37.1	0.90
0.2	0.9	0.92	32.5	0.91	33.9	0.91	0.0	0.91	50.4	0.91	37.1	0.91

[a] See ref 36. The reference weight is the fraction of the electron correlation obtained within the active space. A value significantly different from other species on the PES may indicate an intruder state problem.

The remaining linkage isomer, B−P−C, was not found to be a minimum on either the singlet or triplet PES. Singlet linear B−P−C was observed to be a high-energy transition state between **S2** configurations, whereas the triplet linear B−P−C (**T34**) is a degenerate ($^3\Pi$) Renner−Teller state that connects the **T3** ($^3A'$) and **T4** ($^3A''$) minima (see below for further discussion).

On the triplet surface, there are intruder state problems with **T15** and **T62** at the CASPT2 level. We observed a low reference weight (Rw): 0.15 for **T15** and 0.34 for **T62**. By applying the level shift (LS) technique, we could remove the intrusion and obtain relative energies, as shown in Table 3. When a LS parameter of 0.1 was applied, the problem was solved in **T15** (Rw = 0.90), but **T62** was still affected (Rw = 0.82). With an LS parameter of 0.2, all intruder state problems disappeared. The same shifted values were used to calculate both minima that were connected to each transition state for comparison, and then zero-point energy corrections were applied to obtain the energy differences, relative to **T2**. Finally, we note the strong structural similarity between the diradical transition states **S13** and **T56** ($^1A''$ and $^3A''$) at the DFT and CAS levels. The energy of the triplet **T56** is 15.3 kcal/mol higher than that of **S13** (Figure 2); therefore, intersystem crossing is unlikely.

The singlet and triplet PESs are constructed based on their relative energies after zero-point energy corrections (see Figure 2). As mentioned previously, **S1** is the global minimum. On the singlet PES, **S1** and **S2** are characterized as energy minima. Between **S1** and **S2**, a first-order saddle point, **S12**, is located 18.8 kcal/mol higher than **S1** and 4.8 kcal/mol higher than **S2**. An alternative mechanism for the **S1** → **S2** rearrangement is over the **S13** transition state ($^1A''$) through **S3**, which is the linear P−B−C species. At the UDFT level, **S3** has a $\langle S^2\rangle$ value of 0.56 and no imaginary frequencies. However, at the RDFT level, the energy of the optimized linear structure (**S3′**) is only 1.5 kcal/mol higher than that of the spin-broken symmetry UDFT solution and has two imaginary frequencies (**S2** → **S3′**-(**RDFT**) → **S2**). Although we are not confident that **S3** is an intermediate on the PES, we do feel that the barrier to collapse to **S2** must be very small. In addition, **S2** should undergo rearrangement over a transition state that is very similar to **S3** (i.e., **S3′**(**RDFT**)). In these two scenarios, the P atom can "orbit" the BC fragment (Figure 3). Movement around the C-end gives the global minimum **S1**, whereas movement around the B-end gives the P−BC (**S3**) configuration and then back to **S2**.

The triplet PES is somewhat more complicated than the singlet PES. The triplet surface is composed of $^3A'$, $^3A''$, and $^3\Pi$ states, and all are connected to each other. From the lowest-energy isomer **T2**, the reaction can proceed over a barrier of 17.7 kcal/mol (**T12**) to reach linear **T1** by breaking the B−P bond, over a barrier of 50.4 kcal/mol (**T62**) to reach linear **T6** by breaking the C−P bond, or over a barrier of 77.6 kcal/mol (**T23**) to reach **T3** by breaking the B−C bond. Breaking the C−P bond (**T2** → **T6**) occurs on the $^3A'$ surface to give the

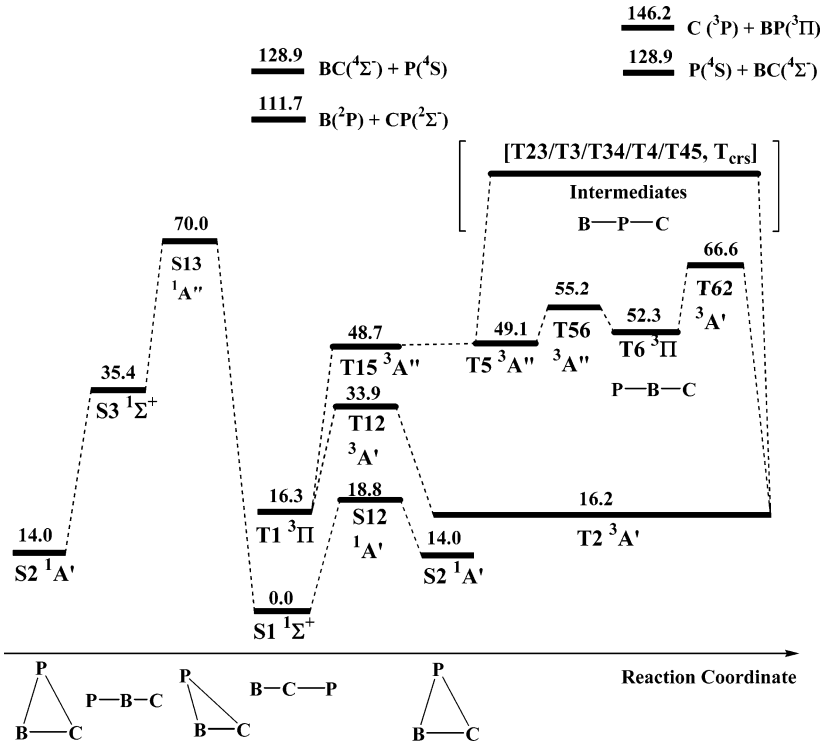

Figure 2. Schematic potential energy surface (PES) for the BCP system. Relative energies (given in kcal/mol) are obtained at the CASPT2+ZPC level. More details of the PES within the square brackets are given in Figure 4.

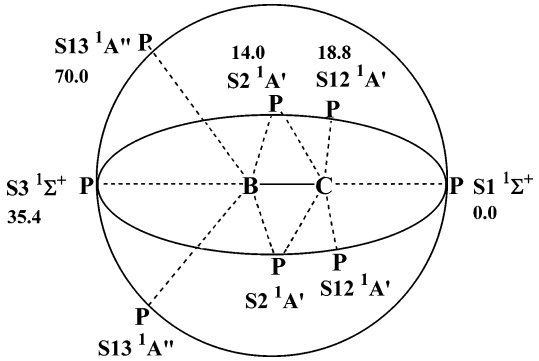

Figure 3. Schematic drawing for revolution of the P atom around the B−C core on the singlet PES. Dashed lines represent the approximate B−C−P angle for the stationary points with the energy (given in kcal/mol), relative to **S1**. The outer circle indicates the A″ surface, whereas the inner eclipse indicates the A′ surface. The A′ and A″ surfaces are degenerate at **S1** and **S3**.

linear P−B−C isomer (**T6**), which can then proceed on a ^{3}A″ surface, because the ^{3}A′ and ^{3}A″ states are degenerate in **T6**. A small barrier of 2.9 kcal/mol (**T56**) separates **T6** from **T5** on the ^{3}A″ surface. From **T5**, the reaction proceeds without any barrier (**T15** is lower in energy than **T5** at the CASPT2+ZPC level).

A higher-energy pathway that connects **T2** and **T1** was calculated; it involves the intermediate species **T3** and **T4** and a crossing point $\mathbf{T_{crs}}$. Although that pathway is not relevant to the **T1**/**T2** pathway, it may be important in reactions between the fragments (BC + P, BP + C, CP + B).

As shown in Figure 4a, the energy of species **T3** (^{3}A′) is 0.3 kcal/mol higher than that of **T34** and 2.2 kcal/mol higher than that of **T4** (**T34**, which is a transition state at the CAS level, is stabilized, relative to **T3** and **T4**, at the CASPT2 level). Similar to the aforementioned **T62**/**T6**/**T56** pathway, the reactant (**T3**) starts on the ^{3}A′ surface and finishes on the ^{3}A″ surface (**T4**) while passing through **T34** (^{3}Π). Distortion along one of the

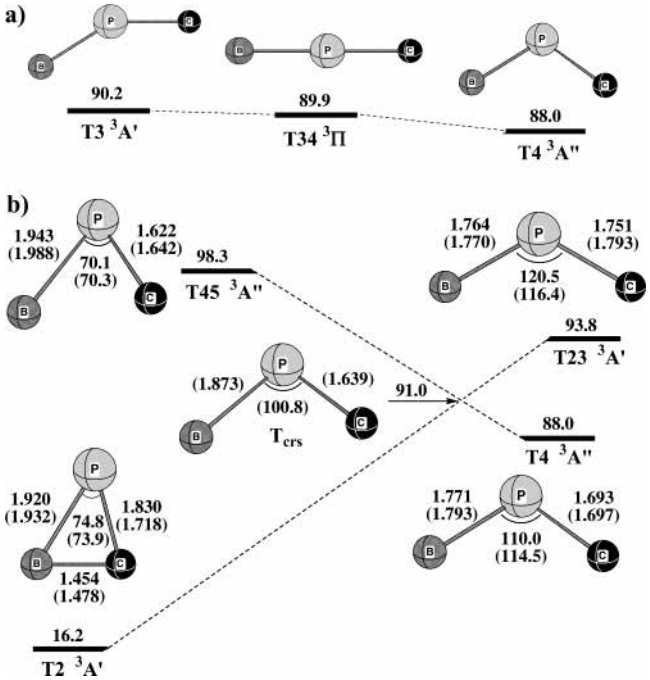

Figure 4. (a) State crossing from the ^{3}A′ surface to ^{3}A″ surface via linear **T34** (^{3}Π). (b) State crossing through a conical intersection; the geometry of $\mathbf{T_{crs}}$ is optimized at the CASSCF(6,6)/6-311+G(2df) level, and single-point calculations were performed for each state symmetry (^{3}A′ and ^{3}A″) at the CASPT2 level. The relative energy of $\mathbf{T_{crs}}$ was obtained by averaging the two state energies. Energies (given in kcal/mol) are relative to **S1**.

two imaginary bending modes (π_x and π_y) of linear B−P−C (**T34**) results in the ^{3}A′ or ^{3}A″ electronic surface.

Another interesting finding in this study is the occurrence of a conical intersection between the ^{3}A′ and ^{3}A″ surfaces. The location is between **T2**−**T23** on the ^{3}A′ surface and **T45**−**T4** on the ^{3}A″ surface (see Figure 4b). The energy of the optimized

TABLE 4: Calculated Bond Dissociation Energies

			D_e (kcal/mol)				D_0 (kcal/mol)		
bond	state	products	DFT	CASPT2	G3B3	experimental	DFT	CASPT2	G3B3
B−C	$^4\Sigma^-$	$^2P + {}^3P$	103.4	102.6	104.3	102.2[a]	101.7	100.9	102.7
C−P	$^2\Sigma+$	$^3P + {}^4S$	123.2	119.9	126.2	123.5[b]	121.3	118.1	124.4
B−P	$^3\Pi$	$^2P + {}^4S$	81.7	72.8	78.4	72.6[c]	80.3	71.4	77.1
B−CP	$^1\Sigma+$	$^2P + {}^2\Sigma^+$	117.4	113.4	118.0		115.7	111.7	116.3
BC−P	$^1\Sigma+$	$^4\Sigma^- + {}^4S$	137.2	130.7	139.8		135.4	128.8	138.0
B−C−P	$^1\Sigma+$	$^2P + {}^3P + {}^4S$	240.6	233.3	244.2		237.0	229.7	240.7

[a] From ref 20. Theoretical values of 97.0 kcal/mol[16] and 100.1 kcal/mol[19] also have been reported. [b] From ref 25. [c] From ref 45.

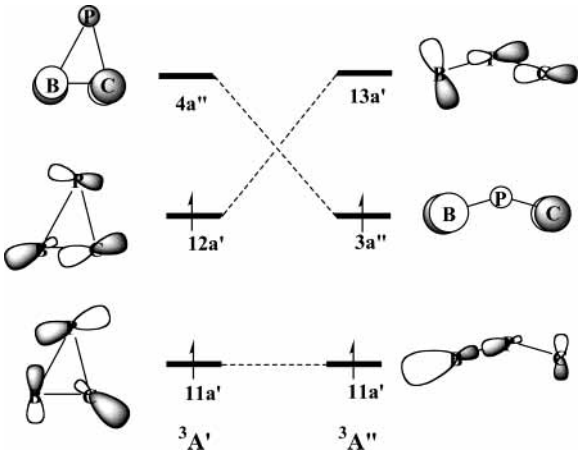

Figure 5. Orbital crossing diagram around the conical intersection (see Figure 4 for details of the crossing).

structure of the crossing point (Figure 4b) is 3.0 kcal/mol higher than that of **T4**. As the B−P−C angle increases, the energy of the ^{3}A′ surface also increases, while the energy of the ^{3}A″ surface decreases. The orbital interactions that are responsible for the crossing are given in Figure 5. When the structure is triangular, the 3a″ orbital has a strong antibonding interaction between the p_z-orbitals of B and C, which decreases as the B−P−C angle increases. At the same time, the bonding interaction in the 12a′ orbital becomes more antibonding as the angle increases. The B−P−C angle at the crossing $\mathbf{T_{crs}}$ (100.8°) is intermediate to the value in **T2** (74.8°) and **T4** (110.0°).

The calculated BDEs are shown in Table 4. Our bond dissociation energy (D_0) of B−C ($^4\Sigma^-$) is 100.9 kcal/mol at the CASPT2 level and 101.7 kcal/mol at the DFT level, which is similar to the experimental value determined by mass spectroscopy ($D_0 = 106 \pm 7$ kcal/mol).[11,12] Tzeli and Marvridis[20] reported MRCI/cc-pVnZ-CBS calculations, including scalar relativistic corrections (mass velocity + Darwin terms) and spin−orbit corrections, and suggested a value of 100.5 ± 0.1 kcal/mol for the B−C bond dissociation energy (D_0). Martin and Taylor[19] used calculations at the CCSD(T) level to obtain a BDE of B−C of 98.3 ± 1 kcal/mol. Our CASPT2 and DFT calculations of the BDE (100.9, 101.7 kcal/mol) are very similar to those reported previously, whereas the G3B3 results give a slightly stronger B−C bond (102.7 kcal/mol).

For the BDE of CP, our DFT results agree best with the reference D_e value of 123.5 kcal/mol,[46] with the CASPT2 calculation being ~4 kcal/mol lower and the G3B3 calculation being ~3 kcal/mol higher than the experimental D_e values. The difference between the CASPT2 and G3B3 methods for the calculated D_e value of CP (as well as for the D_e values of BC and BP) are mainly due to the higher level correction (HLC),[43a] in which deficiencies in the basis set are empirically corrected, based on the number of spin-paired electrons and unpaired α electrons.[47] Without this HLC, the CASPT2 results are very similar to the G3B3 results.

TABLE 5: Wiberg Bond Index, Calculated at the Density Functional Theory (DFT) Level

	Wiberg Bond Index, WBI		
BCP	B−C	C−P	B−P
S1	0.90	2.67	0.14
S2	1.76	1.74	1.16
S3	1.64	0.64	2.33
T1	1.40	2.06	0.16
T2	1.37	1.65	0.92
T3	0.19	2.02	1.53
T4	0.18	1.83	1.51
T5	2.02	0.70	1.34
T6	1.77	0.19	1.85

TABLE 6: NBO Stabilization Energies Associated with Electron Delocalization at the DFT Level

donor	acceptor	energy (kcal/mol)
π_x (C−P)	p_x (B)	13.9
π_y (C−P)	p_y (B)	14.6
σ (B)	σ^* (C−P)	14.3
σ (P)	σ^* (B−C)	16.5

We report the BDEs and atomization energy of BCP (**S1**) in Table 4. Surprisingly, the bond energy (D_e) of B−CP (113.4 kcal/mol, CASPT2) is larger than that in BC (102.6 kcal/mol, CASPT2), even though the DFT-based Wiberg bond index (WBI) of the B−C bond is only 0.90 (Table 5). Also, the bond dissociation energy (D_e) of BC−P (130.7 kcal/mol, CASPT2) is larger than that of the diatomic CP molecule (119.6 kcal/mol, Table 4). These unexpected results can be understood from the WBI and the NBO interaction energy analysis. From the NBO analysis, there is a rather large 1,3-bonding interaction between the B and P atoms (0.14), although their atomic separation is 3.067 Å (DFT). As shown in Table 6, the NBO stabilization energy ("2e-stabilization") between the C−P bonding π-orbitals and empty p-orbitals on B is 28.5 kcal/mol. In addition, the lone-pair electron donations from the B atom to the C−P σ^*-orbital and from the P atom to the B−C σ^*-orbital is stabilizing by 14.3 and 16.5 kcal/mol, respectively. Thus, breaking the B−C bond in BCP also breaks the B···P bonding interaction.

The calculated heats of formation are compared with experimental values in Table 7. In the JANAF table[48] and the NIST Webbook,[49] the heat of formation of BC at 0 K is given as 196 ± 10 kcal/mol, based on the old BDE of BC (105 ± 10 kcal/mol) and heat of formation of boron (132.6 ± 2.9 kcal/mol). Using the newer experimental BDE of BC ($D_e = 102.2$ kcal/mol)[20] with a ZPC correction of 1.7 kcal/mol and a more-recent heat of formation of boron ($\Delta_f H° = 136.2 \pm 0.2$ kcal/mol),[42] we obtained a heat of formation of BC at 0 K as $\Delta_f H° = 206 \pm 1$ kcal/mol, which is in much better agreement with our best results (205.3 kcal/mol, CASPT2 level). DFT and G3B3 results are also in good agreement.

TABLE 7: Heats of Formation of Ground-State Diatomic Fragments and S1

species	$\Delta_f H°$(0 K) (kcal/mol) DFT	CASPT2	G3B3	experimental	$\Delta_f H°$(298 K) (kcal/mol) DFT	CASPT2	G3B3
B				136.2 ± 0.2[a]			
C				169.98 ± 0.1[a]			
P				75.4 ± 0.2[a]			
BC	204.5	205.3	203.5	206 ± 1[b]	206.1	206.8	205.0
CP	124.1	127.3	121.0	124 ± 2[c]	124.6	127.9	121.5
BP	131.3	140.2	134.5		131.9	140.7	135.0
BCP	144.5	151.9	140.9		145.7	153.0	142.1
BCP[d]	145.3	150.5	143.6		146.8	152.1	145.2

[a] From ref 42. [b] Revised, based on the D_e value from Tzeli and Marvridis and the heats of formation of boron and carbon from ref 42. [c] From refs 26−28. [d] Averaged values. See Table 8.

TABLE 8: Heats of Formation of S1 at 0 and 298 K by Different Reactions

reaction	$\Delta_f H°$(0 K) (kcal/mol) DFT	CASPT2	G3B3	$\Delta_f H°$(298 K) (kcal/mol) DFT	CASPT2	G3B3
B + C + P → BCP	144.5	151.9	140.9	145.7	153.0	142.1
BC + P → BCP	146.0	152.6	143.4	148.5	155.0	145.7
B + CP → BCP	144.5	148.5	143.9	146.0	150.0	144.2
BC + CP → BCP + C	146.0	149.2	146.4	146.9	150.2	148.6
average[a]	145.3 ± 0.8	150.5 ± 1.9	143.6 ± 2.2	146.8 ± 1.2	152.1 ± 2.4	145.2 ± 2.7

[a] Error is obtained at the 95% confidence interval.

TABLE 9: Vibrational Frequencies and Renner−Teller Constants of Triplet Linear Species

state	level	Vibrational Frequency (cm^{-1}) π_x	π_y	σ_1	σ_2	Renner−Teller constant, $\lvert\epsilon\rvert$[a]
		Isomer **T1**				
$^3\Pi$	DFT	314.5	225.9	859.6	1577.7	0.319
($^3B_1$)	CAS	326.3	231.3	826.1	1444.0	0.331
		Isomer **T6**				
$^3\Pi$	DFT	273.7	206.7	683.6	1455.4	0.274
($^3B_1$)	CAS	265.0	198.8	671.6	1379.2	0.280
		Isomer **T34**				
$^3\Pi$	DFT	−82.1	−149.5	787.4	940.5	0.537
($^3B_1$)	CAS	−54.8	−142.0	723.2	937.0	0.740

[a] Calculated using the equation $\epsilon = [(\omega^+)^2 - (\omega^-)^2]/[(\omega^+)^2 + (\omega^-)^2]$ in ref 51.

Previous studies have reported a disagreement between theory and experiment for the heat of formation of CP.[26−28] The calculated $\Delta_f H°$(0 K) values for CP—124.1 kcal/mol (DFT), 127.3 kcal/mol (CASPT2), and 121.0 kcal/mol (G3B3)—are in good agreement with the best computational heat of formation (124 ± 2 kcal/mol). The variation between the CASPT2 and G3B3 calculations for the heats of formation (0 K) of CP (6.3 kcal/mol) and BP (5.7 kcal/mol) can be attributed largely to the empirical HLC in the G3B3 method.

The heat of formation of **S1** was calculated in two ways; (i) directly from atoms (B + C + P → BCP) and (ii) by averaging the heats of formation calculated from reactions that are shown in Table 8**,** using reference heats of formation of the reactants. The two methods give similar results at the DFT and CASPT2 levels, but the G3B3 results show more variation. Our best estimate of $\Delta_f H°$(0 K) of BCP ($^1\Sigma^+$) is 150.5 ± 2 kcal/mol at the CASPT2 level.

We note that all three linear triplet species (**T1**, **T6**, and **T34**) have a degenerate electronic state ($^3\Pi$); thus, these are Renner−Teller species.[38] The vibration frequencies of the linear triplet species were calculated at the DFT and CAS levels, to determine the nature of the π bending modes (Table 9). Although a more sophisticated study of the PES is required for a full analysis of the Renner−Teller effect, we note that DFT and CAS give similar results for the π bending modes. Both **T1** and **T6** are RT Type A (i.e., the π modes are different and real)[50] with good agreement between DFT and CAS on the Renner−Teller constant ϵ (see Table 9). The linear triplet **T34** is an RT Type D (i.e., both π modes are different and imaginary) with less agreement on the ϵ value ($\epsilon = 0.54$ via DFT and $\epsilon = 0.74$ via CAS). At the CASPT2 level, there is an indication that **T34** may actually be an RT Type C species (i.e., one π real mode and one π imaginary mode). At the CAS level, **T34** is a transition state between **T3** ($^3A'$) and **T4** ($^3A''$), whereas, at the CASPT2 level, the energy order is **T3**, **T34**, **T4** (i.e., the energy of **T34** is intermediate to that of **T3** and **T4**). Thus, we expect that dynamic electron correlation may have an important effect around this portion of the PES. To clarify this disagreement, we performed a series of CASPT2/ANO-L geometry optimizations[52] for the different electronic states ($^3A'$, $^3A''$, and $^3\Pi$) of **T34** and found that the energy of a slightly bent $^3A'$ state is higher than that of a linear $^3\Pi$ state and the energy of a slightly bent $^3A''$ state is lower than that of the $^3\Pi$ state, thereby confirming that **T34** must be an RT Type C species.

We report the vibrational frequencies and IR intensities for **S1**, **S2**, **T1**, and **T2** calculated at the DFT and CAS levels in Table 10. These are the lowest-energy species on the BCP PESs and may be observable in a low-temperature matrix. The most likely species for observation is **S1**, which has very intense BC and CP IR stretching frequencies.

Conclusions

On the boron−carbon−phosphorus (BCP) potential energy surface (PES), three singlet and six triplet minima were found. The singlet linear BCP (**S1**, $^1\Sigma^+$) is the global minimum, whereas the energies of both the triplet triangular **T2** ($^3A'$) and the triplet linear **T1** are ∼16 kcal/mol higher. Rearrangements of triplets on the $^3A'$ and $^3A''$ PES can occur via two mechanisms: either by going through a linear species of $^3\Pi$ symmetry, where the $^3A'$ and $^3A''$ states are degenerate, or by going through a conical intersection. On the singlet surface, the lowest-energy pathways involve a B−C core with the P atom revolving around the core on the A′ surface **S1** → **S2** → **S3** or on the A″ surface **S1** → **S3**.

Calculation of thermodynamic data at the DFT, CASPT2, and G3B3 levels are in good agreement with each other and with

TABLE 10: Calculated Vibrational Frequencies and IR Intensities of S1, S2, T1, and T2[a]

	DFT	CAS
	S1	
ν_1	130.0 (9.2)	180.7 (3.5)
ν_2	135.3 (9.7)	180.7 (3.5)
ν_3	739.2 (20.4)	714.6 (122.7)
ν_4	1449.6 (23.0)	1466.8 (341.6)
	S2	
ν_1	606.6 (21.7)	645.6 (75.2)
ν_2	929.6 (21.7)	885.9 (40.0)
ν_3	1308.4 (16.3)	1350.0 (16.4)
	T1	
ν_1	225.9 (5.9)	231.3 (3.5)
ν_2	314.5 (16.1)	326.3 (11.2)
ν_3	859.6 (0.3)	826.1 (0.6)
ν_4	1577.7 (52.1)	1444.0 (15.2)
	T2	
ν_1	590.6 (19.8)	594.9 (15.2)
ν_2	932.3 (8.8)	892.8 (7.3)
ν_3	1243.8 (10.2)	1193.2 (7.5)

[a] Vibrational frequencies (in units of cm^{-1}) are given in regular type. IR intensities (in units of km/mol) are given in parentheses.

experimental values. The B−C and C−P bond dissociation energies (D_0) in B−C−P are 111.7 and 128.9 kcal/mol by CASPT2, respectively, which are larger than the bond dissociation energies in the BC and CP diatomics (100.9 and 118.1 kcal/mol, respectively). The stronger B−C and C−P bonds in BCP are due to stabilizing 1,3-interactions between the B and P atoms. The calculated heat of formation ($\Delta_f H°$) of BCP ($^1\Sigma^+$) is 150.5 ± 2 kcal/mol at the CASPT2 level. The absence of other low-energy unimolecular reactions suggests that BCP might be observed under appropriate conditions.

Three Renner−Teller species among the BCP isomers are discussed. Two of them (**T1** and **T6**) are classified as an RT Type A species, and the other isomer (**T34**) is classified as a Type C species. In analogy with the boron−carbon−nitrogen (BCN) monomer and BCN polymeric materials, we hope that this study of the BCP monomer may contribute to its discovery or to the search for BCP polymer materials. To this end, studies of polymers that are based on the BCP monomer unit are underway.

Acknowledgment. Computer time was made available on the Auburn COSAM PRISM cluster. We thank Dr. Ohyun Kwon for helpful conversations.

References and Notes

(1) Aoki, K.; Tanaka, S.; Tomitani, Y.; Yuda, M.; Shimada, M.; Oda, K. *Chem. Lett.* **2002**, 112.

(2) Kawano, T.; Kawaguchi, M.; Okamoto, Y.; Enomoto, H.; Bando, H. *Solid State Sci.* **2002**, *4*, 1521.

(3) Langenhorst, F.; Solozhenko, V. L. *Phys. Chem. Chem. Phys.* **2002**, *4*, 5183.

(4) Ahn, J. Y.; Yoon, S. F.; Zhang, Q.; Gan, R. B.; Chew, K.; Yu, M. B.; Bai, X. D.; Wang, E. G. *Appl. Phys. Lett.* **2000**, *77*, 1949.

(5) Gago, R.; Jimenez, I.; Agulló-Rueda, F.; Albella, J. M.; Czigány, Z.; Hultman, L. *J. Appl. Phys.* **2002**, *92*, 5177.

(6) Miyamoto, Y.; Rubio, A.; Cohen, M. L.; Louie, S. G. *Phys. Rev. B* **1994**, *50*, 4976.

(7) Thomson, C. *J. Chem. Phys.* **1973**, *58*, 216.

(8) Martin, J. M. L.; Tayler, P. R. *J. Phys. Chem.* **1994**, *98*, 6105.

(9) Lanzisera, D. V.; Andrews, L. *J. Phys. Chem. A* **1997**, *101*, 9660.

(10) Lanzisera, D. V.; Andrews, L.; Taylor, P. R. *J. Phys. Chem. A* **1997**, *101*, 7134.

(11) Verhaegen, D. G.; Stafford, F. E.; Ackerman, M.; Drowart, J. *Nature* **1962**, *193*, 1280.

(12) Verhaegen, D. G.; Stafford, F. E.; Drowart, J. *J. Chem. Phys.* **1964**, *40*, 1662.

(13) Kuoba, J. E.; Öhrn, Y. *J. Chem. Phys.* **1970**, *53*, 3923.

(14) Fernando, W. T. M. L.; O'Brien, L. C.; Bernath, P. F. *J. Chem. Phys.* **1990**, *93*, 8482.

(15) Wyss, M.; Grutter, M.; Maier, J. P. *J. Phys. Chem. A* **1998**, *102*, 9106.

(16) Hirsch, G.; Buenker, R. J. *J. Chem. Phys.* **1987**, *87*, 6004.

(17) Knight, L. B., Jr.; Cobranchi, S. T.; Petty, J. T.; Earl, E.; Feller, D.; Davidson, E. R. *J. Chem. Phys.* **1989**, *90*, 690.

(18) Oliphant, N.; Adamowicz, L. *Chem. Phys. Lett.* **1990**, *168*, 126.

(19) Martin, J. M. L.; Taylor, P. R. *J. Chem. Phys.* **1994**, *100*, 9002.

(20) Tzeli, D.; Mavridis, A. *J. Phys. Chem. A* **2001**, *105*, 1175.

(21) Kumashiro, Y.; Sato, K.; Chiba, S.; Yamada, S.; Tanaka, D.; Hyodo, K.; Yokoyama, T.; Hirata, K. *J. Solid State Chem.* **2000**, *154*, 39.

(22) Ferhat, M.; Zaoui, A.; Certier, M.; Aourag, H. *Physica B* **1998**, *252*, 229.

(23) Rodríguez-Hernández, P.; González-Diaz, M.; Muñoz, A. *Phys. Rev. B* **1995**, *51*, 14705.

(24) Zaoui, A.; Hassan, F. E. H. *J. Phys.: Condens. Matter* **2001**, *13*, 253.

(25) (a) de Brouckère, G.; Feller, D. *J. Phys. B: At. Mol. Opt. Phys.* **1996**, *29*, 5283. (b) Fast, P. L.; Sánchez, M.; Truhlar, D. G. *J. Chem. Phys.* **1999**, *111*, 2921.

(26) Fleming, P. E.; Lee, E. P. F.; Wright, T. G. *Chem. Phys. Lett.* **2000**, *332*, 199.

(27) Kwon, O.; McKee, M. L. *J. Phys. Chem. A* **2001**, *105*, 478.

(28) Hajgató, B.; Pham-Tran, N.; Veszprémi, T.; Nguyen, M. T. *Phys. Chem. Chem. Phys.* **2001**, *3*, 5158.

(29) Frisch, M. J.; Trucks, G. W.; Schlegel, H. B.; Scuseria, G. E.; Robb, M. A.; Cheeseman, J. R.; Zakrzewski, V. G.; Montgomery, J. A., Jr.; Stratmann, R. E.; Burant, J. C.; Dapprich, S.; Millam, J. M.; Daniels, A. D.; Kudin, K. N.; Strain, M. C.; Farkas, O.; Tomasi, J.; Barone, V.; Cossi, M.; Cammi, R.; Mennucci, B.; Pomelli, C.; Adamo, C.; Clifford, S.; Ochterski, J.; Petersson, G. A.; Ayala, P. Y.; Cui, Q.; Morokuma, K.; Salvador, P.; Dannenberg, J. J.; Malick, D. K.; Rabuck, A. D.; Raghavachari, K.; Foresman, J. B.; Cioslowski, J.; Ortiz, J. V.; Baboul, A. G.; Stefanov, B. B.; Liu, G.; Liashenko, A.; Piskorz, P.; Komaromi, I.; Gomperts, R.; Martin, R. L.; Fox, D. J.; Keith, T.; Al-Laham, M. A.; Peng, C. Y.; Nanayakkara, A.; Challacombe, M.; Gill, P. M. W.; Johnson, B.; Chen, W.; Wong, M. W.; Andres, J. L.; Gonzalez, C.; Head-Gordon, M.; Replogle, E. S.; Pople, J. A. *Gaussian 98*, revision A.11; Gaussian, Inc., Pittsburgh, PA, 2001.

(30) (a) Becke, A. D. *J. Chem. Phys.* **1993**, *98*, 5648. (b) Lee, C.; Yang, W.; Parr, R. G. *Phys. Rev. B* **1988**, *37*, 785. (c) Miehlich, B.; Savin, A.; Stoll, H.; Preuss, H. *Chem. Phys. Lett.* **1989**, *157*, 200.

(31) Schmidt, M. W.; Baldridge, K. K.; Boatz, J. A.; Elbert, S. T.; Gordon, M. S.; Jensen, J. J.; Koseki, S.; Matsunaga, N.; Nguyen, K. A.; Su, S.; Windus, T. L.; Dupuis, M.; Montgomery, J. A. GAMESS. *J. Comput. Chem.* **1993**, *14*, 1347.

(32) Roos, B. O. The Complete Active Space Self-Consistent Field Method and Its Applications in Electronic Structure Calculations. In *Advances in Chemical Physics: Ab Initio Methods in Quantum Chemistry—II*; Lawley, K. P., Ed. Wiley: Chichester, U.K., 1987.

(33) Andersson, K.; Barysz, M.; Bernhardsson, A.; Blomberg, M. R. A.; Cooper, D. L.; Fülscher, M. P.; de Graaf, C.; Hess, B. A.; Karlström, G.; Lindh, R.; Malmqvist, P.-Å.; Nakajima, T.; Neogrády, P.; Olsen, J.; Roos, B. O.; Schimmelpfennig, B.; Schütz, M.; Seijo, L.; Serrano-Andrés, L.; Siegbahn, P. E. M.; Stålring, J.; Thorsteinsson, T.; Veryazov, V.; Widmark, P.-O. MOLCAS Version 5.4, Lund University, Lund, Sweden, 2002.

(34) (a) Roos, B. O.; Andersson, K.; Fülscher, M. P.; Malmqvist, P.-Å.; Serrano-Andrés, L.; Pierloot, K.; Merchán, M. Multiconfigurational Perturbation Theory: Applications in Electronic Spectroscopy. In *Advances in Chemical Physics: New Methods in Computational Quantum Mechanics*; Prigogine, I., Rice, S. A., Eds.; Wiley: New York, 1995. (b) Andersson, K.; Malmqvist, P.-Å.; Roos, B. O.; Sadlej, A. J.; Wolinski, K. *J. Phys. Chem.* **1990**, *94*, 5483. (c) Andersson, K.; Malmqvist, P.-Å.; Roos, B. O. *J. Phys. Chem.* **1992**, *96*, 1218.

(35) (a) Krishnan, R.; Binkley, J. S.; Seeger, R.; Pople, J. A. *J. Chem. Phys.* **1980**, *72*, 650. (b) McLean, A. D.; Chandler, G. S. *J. Chem. Phys.* **1980**, *72*, 5639. (c) Clark, T.; Chandrasekhar, J.; Spitznagel, G. W.; Schleyer, P. v. R. *J. Comput. Chem.* **1983**, *4*, 294.

(36) (a) Roos, B. O.; Andersson, K. *Chem. Phys. Lett.* **1995**, *245*, 215. (b) Roos, B. O.; Andersson, K.; Fülscher, M. P.; Serrano-Andrés, L.; Pierloot, K.; Merchán, M.; Molina, V. *THEOCHEM* **1996**, *388*, 257.

(37) Schaftenaar, G.; Noordik, J. H. MOLDEN. *J. Comput.-Aided Mol. Des.* **2000**, *14*, 123.

(38) (a) Renner, R. *Z. Phys.* **1934**, *92*, 172. (b) Herzberg, G. *Molecular Spectra and Molecular Structure III. Electronic Spectra and Electronic Structure of Polyatomic Molecules*; Krieger: Malabar, FL, 1991.

(39) (a) Widmark, P. O.; Malmqvist, P.-Å.; Roos, B. O. *Theor. Chim. Acta* **1990**, *77*, 291. (b) Widmark, P. O.; Malmqvist, P.-Å.; Roos, B. O. *Theor. Chim. Acta* **1991**, *79*, 419.

(40) Reed, A.; Curtiss, L. A.; Weinhold, F. *Chem. Rev.* **1988**, *88*, 899.
(41) Wiberg, K. B. *Tetrahedron* **1968**, *24*, 1083.
(42) (a) Ochterski, J. W. *Thermochemistry in Gaussian*, Gaussian White Paper. (Available on the Internet at http://www.Gaussian.com/g_whitepap/thermo.htm.) (b) Curtiss, L. A.; Raghavachari, K.; Redfern, P. C.; Pople, J. A. *J. Chem. Phys.* **1997**, *106*, 1063.
(43) (a) Curtiss, L. A.; Raghavachari, K.; Redfern, P. C.; Rassolov, V.; Pople, J. A. *J. Chem Phys.* **1998**, *109*, 7764. (b) Baboul, A. G.; Curtiss, L. A.; Redfern, P. C.; Raghavachari, K. *J. Chem. Phys.* **1999**, *110*, 7650.
(44) Boldyrev, A. I.; Simons, J. *J. Chem. Phys.* **1993**, *97*, 6149.
(45) Miguel, B.; Omar, S.; Mori-Sánchez, P.; García de la Vega, J. M. *Chem. Phys. Lett.* **2003**, *381*, 720.
(46) Huber, K. P.; Herzberg, G. *Molecular Spectra and Molecular Structure. IV. Constants of Diatomic Molecules*; Van Nostrand: New York, 1979.
(47) We calculated ΔE(HLC) as found in ref 43a. The resulting $\Delta\Delta E$(HLC) values for diatomic fragments are as follows: BC, 3.6 kcal/mol; CP, 6.4 kcal/mol; BP, 5.0 kcal/mol. These corrections increase the bond dissociation energies computed by the G3B3 method. When this factor is taken into consideration, the CASPT2 and G3B3 methods give very similar bond dissociation energies.
(48) Chase, M. W., Jr. NIST−JANAF Thermochemical Tables, 4th ed. *J. Phys. Chem. Ref. Data* **1998**, Monograph 9.
(49) NIST Chemistry Webbook Site, http://webbook.nist.gov/chemistry.
(50) Lee, T. J.; Fox, D. J.; Schaefer, H. F.; Pitzer, R. M. *J. Chem. Phys.* **1984**, *81*, 356.
(51) Brown, S. T.; Yamaguchi, Y.; Schaefer, H. F. *J. Phys. Chem. A* **2000**, *104*, 3603.
(52) For a discussion of CASPT2 optimized geometries, see: Page, C. S.; Olivucci, M. *J. Comput. Chem.* **2003**, *24*, 298.